Effect of the Strain Rate and Microstructure on Damage Growth in Aluminum

R. R. Valisetty[1], A.M. Dongare[2], A.M. Rajendran[3], R. R. Namburu[1]

Abstract: Materials used in soldier protective structures, such as armor, vehicles and civil infrastructures, are being improved for performance in extreme dynamic environments. Nanocrystalline metals show significant promise in the design of these structures with superior strengths attributed to the dislocation-based and grain-boundary-based processes as compared to their polycrystalline counterparts. An optimization of these materials, however, requires a fundamental understanding of damage evolution at the atomic level. Accordingly, atomistic molecular dynamics simulations are performed using an embedded-atom method (EAM) potential on three nano-crystalline aluminum atom systems, one a Voronoi-based nano-crystalline system with an average grain size of 10 nm, and the other two single crystals. These simulations are performed under the condition of uniaxial expansion at several strain rates ranging from $10^6 s^{-1}$ to 10^{10} s^{-1}. Results for the effective stress are discussed with the aim of establishing the role of the strain rate and microstructure on the evolution of the plastic strain and void volume fraction and the eventual loss of stress carrying capability of the atom systems.

Keywords: Nanocrystalline metals; Molecular dynamics; Voids, Dynamic failure.

1   Introduction

Most tensile failures occur in ductile materials due to the evolution of micro voids from nucleation growth, to coalescence. When the stress state is highly triaxial under tension such as in the necked regions of quasi-static uniaxial tension specimens, voids grow as spherical and specimens fracture due to voids coalescence. Spallation [Knott (1973)] is a dynamic tensile fracture that occurs under high triaxial stress conditions in plate impact experiments [Curran, Seaman and Shockey

---

[1] Army Research Laboratory, Comp. & Info. Sciences Directorate, APG, MD 21005.

[2] Department of Chem., Mat. & Biomol. Engg., Univer. Connecticut, Storrs, CT 06269.

[3] Department of Mech. Engineering, University of Mississippi, University, MS 38677.
 ramakrishna.r.valisetty.civ@mail.mil, dongare@uconn.edu

(1987)] wherein a flyer-plate is impacted on to a target plate at a very high velocity. The material typically experiences strain rates in the range of 10^5 to 10^7/sec. The impact initially generates compressive waves in the plates which upon reflection from stress free lateral surfaces become tensile and interact with each other producing a triaxial stress state in the spall regions of the target plate. Multiple voids are observed to nucleate in this region which grow and coalesce to form microscopic cracks

Research over the past few decades via experiments suggested that the voids in ductile materials were generally observed to be almost spherical in shape and nucleate at grain boundaries due to grain boundary sliding and/or dislocation pileups during impact loading [Curran, Seaman, and Shockey (1987)]. Most spall experiments were aimed at evaluating the spall strength (peak tensile pressure prior to failure) of the material and understanding the effects of the microstructure and loading conditions on the void nucleation, while understanding of growth and coalescence of voids at the onset of spall failure is still in its infancy. Even though peak strain rates of $10^5 s^{-1}$ to $10^6 s^{-1}$ are achieved in the plate impact experiments [Curran, Seaman, and Shockey (1987); Minich, Cazamias, Kumar, and Schwartz (2004); Rivas, Zurek, Thissell, Tonks, and Hixson (2000); Fowler, Worswick, Pilkey, and Nahme (2000)], and peak strain rates of $10^7 s^{-1}$ to $10^9 s^{-1}$ in the laser-shock experiments [Tamura, Kohama, Kondo, and Yoshida (2001); Moshe, Eliezer, Dekel, Ludmirsky, Henis, Werdiger, Goldberg, Eliaz, and Eliezer (1998); Moshe, Eliezer, Dekel, Henis, Ludmirsky, Goldberg, and Eliezer (1999); Kanel, Razorenov, Utkin, Fortov, Baumung, Karow, Rusch, and Licht (1993); Eliezer, Gilath, and Bar-Noy (1990); Meyers (1994)], the underlying deformation is controlled by small time scales which makes it difficult to identify and characterize the fracture processes using experiments alone.

During 80s, the ductile failure in solids has been extensively studied using yield functions [Gurson (1977); Tvergaard and Needleman (1984)] developed to address the mechanism of void growth and porosity for porous materials. For instance, [Rajendran and Fyfe (1982)] employed a yield function in their material model to predict the failure strains in aluminum and copper at high strain rates under uniaxial stress state. There are several review articles on modeling of spall failure using such yield functions in open literature [Kanel, Seaman, and Antoun (2003)]. A few spall-failure theories were developed [Rajendran, Dietenberger, and Grove (1989); Thomason (1999); Wright and Ramesh (2008)] by describing effects of strain rates and microstructure on nucleation, growth, and coalescence by making some assumptions. Almost all continuum models that described the nucleation and growth of voids and their effects on the degradation of strength in solids under both quasi-static and dynamic loading conditions were either empirically or mi-

cromechanically based. The model parameters to describe the failure processes were mostly adjusted to fit some experimental measurements. These models often require estimating several parameters that cannot be directly measured from any dynamic experiments.

In general, from the extensive metallographic analyses on the recovered specimens, the dynamic failure process events of the void nucleation, growth and coalescence were inferred, and were introduced into the continuum models with the aid of approximations. The voids nucleation and growth were modeled through the evolution of some state variables, such as cumulative damage or void volume fraction (V_f). Due to the advent of computer capabilities in the last decade, it is now possible to perform molecular dynamics (MD) simulations that may provide an atomic level detail needed for the physical understanding and interpretation of evolution of voids, especially the nucleation process. Since spallation like failure occurs the very high strain rates, the MD simulations are naturally suitable for analyzing at atomic scale micromechanisms in spall failure. If the void growth based mechanisms are present across all atomistic, micro, and macro scales, then it may be possible to seamlessly bridge the scales. The fact that the strain rates are similar in all scales allows for investigating the results of the MD simulations for insights into the void growth mechanisms which in turn may help gain a better understanding of the results from the high strain rate experiments and later to come up with better models for improving the finite element/difference based continuum modeling, MD simulations are now coupled with continuum modeling via cost effective methods e.g., the meshless local Petrov-Galerkin (MLPG) method [Atluri and Shen (2002); Shen, and Atluri (2004a)], the lattice Green function method [Tewary and Read (2004)], the 3D T-Trefftz Voronoi cell based finite element method [Dong, and Atluri (2012)]

MD simulations have been employed to study the void growth mechanisms in single-crystal systems [Seppala, Belak, and Rudd (2004); Dongare, Rajendran, LaMattina, Zikry, and Brenner (2008); Traiviratana, Bringa, Bensona, and Meyers (2008)], and void coalescence [Seppala, Belak, and Rudd (2004); Seppala, Belak, and Rudd (2005)] for loading conditions on the spall plane at strain rates $\geq 10^8 \text{s}^{-1}$. But for the existence of some pre-selected voids, the initial systems in these studies were damage-free and defect-free single crystal systems. Thus, the micro-mechanisms related to nucleation of voids were neglected in these simulations. The MD simulations of deformation suggested that void growth occurred through the heterogeneous nucleation of dislocations from a void surface. In addition, the simulations also suggested that two neighboring voids coalesced through a development of slip planes between the voids.

MD studies recently have been also used to investigate the void nucleation mech-

anisms in nanocrystalline Cu [Dongare, Rajendran, LaMattina, Zikry, and Brenner (2009b)] for an uniaxial tensile strain condition at a constant strain rate of $10^8 s^{-1}$ and under shock loading [Dongare, Rajendran, LaMattina, Zikry, and Brenner (2010a)]. These studies suggested that the presence of a large volume fraction of grain boundaries had significant effect on the void nucleation and growth Triple junctions of grain boundaries were seen to be significant sources for void nucleation and their growth along the grain boundaries. The void nucleation mechanisms were attributed to mechanical separation/sliding at triple junction points, which were in contrast to the dislocation pile-ups observed in polycrystalline metals. The void nucleation was observed to cause a shell of disordered material to surround the void and further growth of the voids was reported to occur by the shearing of the neighboring disordered material. This mechanism resulted in a fast growth of the voids, following the initial void nucleation. During this phase the temperature of the system increased which in turn, resulted in the recrystallization of the disordered material. The recrystallization of the surrounding material resulted in a slower subsequent growth of the voids. The simulations [Dongare, Rajendran, LaMattina, Zikry, and Brenner (2009b), Dongare, Rajendran, LaMattina, Zikry, and Brenner (2010a)] therefore demonstrated two additional stages of void growth following the initial void nucleation under uniaxial tensile strain in nanocrystalline Cu at a constant strain rate of $10^8 s^{-1}$.

Recently [Dongare, Rajendran, LaMattina, Zikry, and Brenner (2011)] have extended their study to include a loading strain rate range of $4 \times 10^7 s^{-1} - 10^{10} s^{-1}$ and a grain size range of 6–12 nm. They reported that the spall strength of the nanocrystalline Cu to be strongly dependent on the strain rate and less dependent on the grain size in the inverse Hall-Petch regime. The spall strength was observed to increase with increasing strain rate and resulted in delayed failure They also reported a power-law dependence of the nucleation of voids as well as the time for nucleation of voids of nanocrystalline Cu at high strain rates.

An Al microstructure with grains is considered in the present paper. The objective is to investigate how grains with an average grain size of 10 nm affect the nucleation and void growth for uniaxial strain loading under strain rates ranging from $10^6 s^{-1}$-$10^{10} s^{-1}$. The nucleation, growth, and coalescence of voids are considered in terms of the evolution of V_f, plastic strain (ε_p) and total number of voids or void totals (N_v), and compared with simulations from two pure perfect face centered cubic (fcc) based Al single crystal atom systems. The results suggest that the loading strain rates have a strong influence on the evolution of the voids and the voids subsequently affect the flow stress (von Misses or effective stress) and spall strength in the nanocrystalline Al. On the other hand, the presence of grains reduces these strengths by offering the GB junctions as readily convenient sites for the initial void

nucleation. The computational details are presented in Section 2. The effects of the microstructure and loading strain rates on the stress-strain profiles are discussed in Section 3.1, and the void evolution in Section 3.2. The relevance of the results to modeling the Al spall behavior is discussed in Section 4

2   Computational Details

2.1   *Atom systems and MD simulations*

In addition to void growth, MD simulations may be used in studying various hardening mechanisms in atom systems including the effects of dopants on properties of thin films [Xiong, and Chen (2008)], and of includsions [Dong, and Atluri (2012)]. The present MD simulations are conducted using the LAMMPS code [Plimpton, (1995)] and the embedded atom method (EAM) potential of [Mishin, Farkas, and Mehl (1999)]. This EAM potential is well suited for modeling nano-crystalline Al as it provides a good description of the material failure behavior [Voter (1994); Tsuru, and Shibutani (2004)]. The present study focuses on the dynamic failure behavior of three Al atom systems. As shown in Figure 1 the first one is a 10 nm nanocrystalline aluminum (NCA) atom system. It contains a total of 3,744,842 atoms in 122 grains with an average grain size of 10 nm and is constructed using Voronoi-based tessellation. It is a cube with the overall box dimensions of 39.9 nm x 39.9 nm 39.9 nm. The second and third systems are single crystal aluminum (SCA) atom systems; they are based on the fcc lattice structure with a lattice constant of 4.05 Å. These two systems are used for comparing and contrasting the role of the 10nm grain microstructure in the NCA atom system. The second atom system, or the 1st SCA atom system, contains a total of 3,881,196 atoms. It is constructed in the form of a cube with a side length of 40.24 nm. This one is comparable both in size and in number of atoms to the NCA atom system. The third atom system, or the 2nd SCA atom system, contains 614,656 atoms in a rectangular solid shape of the following box dimensions: 260.4 nm x 199.19 nm x 199.19 nm. As the MD simulations take a very long time at lower strain rates, the third system was considered with a smaller number of atoms.

Prior to applying the uniaxial strain condition, all the atom systems were equilibrated to have zero pressure at 300K for 350 ps using a computational statistical equilibrium procedure and a temperature rescaling procedure of the LAMMPS code. Periodic boundary conditions were applied in all the three directions. Then, using an additional procedure, called "erate" procedure in the LAMMPS code, the strain rates were applied by increasing the atom systems' box dimensions incrementally in the direction of the overall strain while keeping the lateral dimension fixed so as to impose an uniaxial tensile strain loading condition. While the uni-
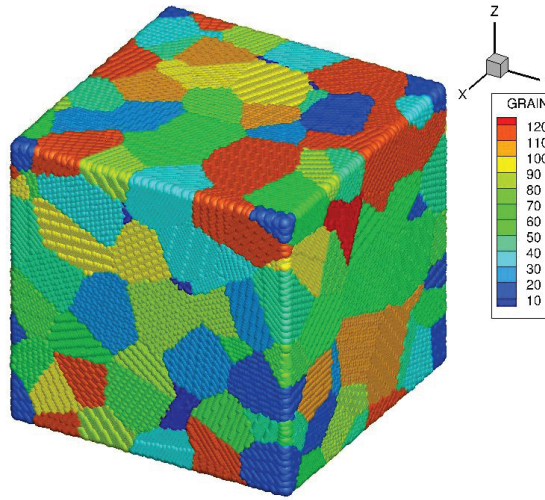
Figure 1: The initial configuration of NCA atom system with 122 grains with an average grain size of 10 nm. The atoms are colored according to the grain number which is arbitrary.

axial expansion is applied in the <1,0,0> direction of the atom lattice structure for the SCA atom systems, the expansion direction cannot be associated with any particular lattice direction for the NCA atom system because the system contains grains oriented in arbitrary directions. For the 2nd SCA atom system, the expansion direction also coincides with the longer dimension of the box. The engineering definition is used for the strains; they are computed from changes in the atom systems' overall box dimension in the strain rate direction. As the systems' box dimensions are incremented, equilibriums of the atom systems were secured using a statistical equilibrium procedure of the LAMMPS code. Time steps in the range of 0.001 to 0.002 ps were used.

2.2 Stress and strain responses

The elements of the atomic-level stress tensor were calculated as

$$\sigma_{\alpha\beta} = -\frac{1}{\Omega_0}\left[\frac{1}{2}\sum_j F_{ij}^\alpha r_{ij}^\beta + M_i v_i^\alpha v_j^\beta\right] \tag{1}$$

where α and β denote the Cartesian coordinates, Ω_0 is the atomic volume, F_{ij} is the force on atom i due to atom j, M_j is the mass of atom i, and v_i is the velocity of atom i. While, a recently developed atomic-level stress tensor [Shen and Atluri (2004b)]

proves to be more accurate under conditions of non-homogeneous deformation, it is assumed that the current simulation results will not change significantly for the uniform deformation conditions of uniaxial tensile strain. When this stress tensor is averaged over all the atoms of an atom system, the average stresses,σ_x, σ_y, σ_z emerge, from which the mean stress (σ_m), the flow stress (σ_e) and the effective von Mises strain (ε_e) were computed as follows:

$$\sigma_m = \frac{1}{2}(\sigma_x + \sigma_y + \sigma_z) \tag{2}$$

$$\sigma_e = \sqrt{\frac{1}{2}[(\sigma_x - \sigma_y)^2 + (\sigma_y - \sigma_z)^2 + (\sigma_z - \sigma_x)^2]} \tag{3}$$

$$\varepsilon_e = \sqrt{\frac{2}{9}[(\varepsilon_x - \varepsilon_y)^2 + (\varepsilon_y - \varepsilon_z)^2 + (\varepsilon_z - \varepsilon_x)^2]} \tag{4}$$

2.3 *Damage responses*

In addition to the mechanical responses of stress and strain, damage in the atom systems was investigated in terms of three response parameters: void volume fraction (V_f), plastic strain (ε_p) and void totals (N_v) or the total number of voids in each system. To have a quantitative understanding of the effect of microstructure on the void growth behavior, the evolutions of V_f, ε_p, N_v were monitored during the straining. V_f was defined as the ratio of the total volume of the voids (V_v) to the total volume (V_{tot}) of the atom system. To calculate V_f, a three-dimensional grid of cubic cells was superimposed over the deforming atom system and clusters of two or more contiguous empty cells were identified as voids [Zhigilei, Ivanov, Leveugle, Sadigh, and Bringa (2004); Dongare, Rajendran, LaMattina, Zikry, and Brenner (2009b)]. The total volume of the empty cells divided by the volume of the atom system is calculated as the void fraction. After exploring from 3.7 nm to 4.06 nm, a cell size of 4.06 nm was chosen to ensure at least several atoms in the cell for the case without any voids.

The ε_p is calculated assuming that the current total strain increment can be separated into elastic and plastic components as

$$d\varepsilon_{tot} = \dot{\varepsilon}_{tot}\, dt = \dot{\varepsilon}_{el}\, dt + \dot{\varepsilon}_{pl}\, dt \tag{5}$$

For the an application of uniaxial strain in z direction, the general form of Hooke's law enables the computation of current stress increments as

$$\begin{aligned}
d\sigma_x &= \lambda\, \dot{\varepsilon}\, dt \\
d\sigma_y &= \lambda\, \dot{\varepsilon}\, dt \\
d\sigma_z &= (\lambda + 2\mu)\, \dot{\varepsilon}\, dt,
\end{aligned} \tag{6}$$

where, λ and μ are the Lame's constants. From Equations (5) and (6), the current ε_p increment was computed as

$$\dot{\varepsilon}_{pl}\, dt = \dot{\varepsilon}_{tot}\, dt - \frac{\sigma_x + \sigma_y + \sigma_z}{3\lambda + 2\mu} \tag{7}$$

3   Dynamic failure: Effects of the strain rate and microstructure on aggregate responses

Large scale MD simulations of uniaxial expansion were conducted for all the three atom systems. The nanocrystalline aluminum (NCA) atom system with 10nm grains was subjected to the following strain rates: 10^6s^{-1}, 10^7s^{-1}, 10^8s^{-1}, 10^9s^{-1} and 10^{10}s^{-1}. The 1st single crystal aluminum (SCA) atom system was subjected to the following strain rates: 10^7s^{-1}, 10^8s^{-1}, 10^9s^{-1} and 10^{10}s^{-1}, and the 2nd SCA atom system to 10^6s^{-1}. As the MD simulations take a very long time for the smaller strain rates, the 2nd SCA atom system, which is smaller than the 1st SCA system, was considered and used for generating the results for the strain rate of 10^6s^{-1}. One of the important aspects of the present simulations is obtaining the MD results for the NCA system for the strain rate of 10^6s^{-1} which approaches the strain rates measured in conventional shock wave based plate impact experiments. The simulations yielded two types of results: 1. overall on the atom aggregates, the average responses of stress, strain, ε_p, and V_f, and 2. within the atom systems themselves, the evolution of damage which in the present study is considered in the form of N_v, the total number of voids for each atom system. Both types of results are affected by the strain rate and by the presence of the grains, but the discussion about the damage evolution, in the present study, was limited to the overall V_f.

3.1   Flow stress, its initial development and its maximum values

The flow stress (σ_e) curves are presented in Figure 2(a) for the NCA and in Figure 2(b) for the two SCA atom systems as a function of the applied strain for strain rates 10^6s^{-1}, 10^7 s^{-1}, 10^8 s^{-1}, 10^9 s^{-1} and 10^{10} s^{-1}. The same results are presented in Figures 2(c) and 2(d) using an expanded scale for the applied strain to highlight the strain rate effect on the initial development of σ_e in the loading process. The strain rate has an effect of increasing the σ_e for both the NCA and SCA atom systems. It further has an effect of significantly increasing the strain hardening for the NCA atom system than for the two SCA systems. A slight strain rate dependency can be observed for strain rates above 10^8/sec, however, in the SCA systems as they continue to strain harden up to 12%-14% strain. This strain hardening behavior terminates at 6% strain in the NCA system. The maximum σ_e, taken at all of the 5 strain rates, reaches a range of 4.13-4.34 GPa and an average value of 4.23 GPa in

the SCA systems, but the in the NCA system, it reaches a range of only 0.88-1.73 GPa and an average of 1.22 GPa.
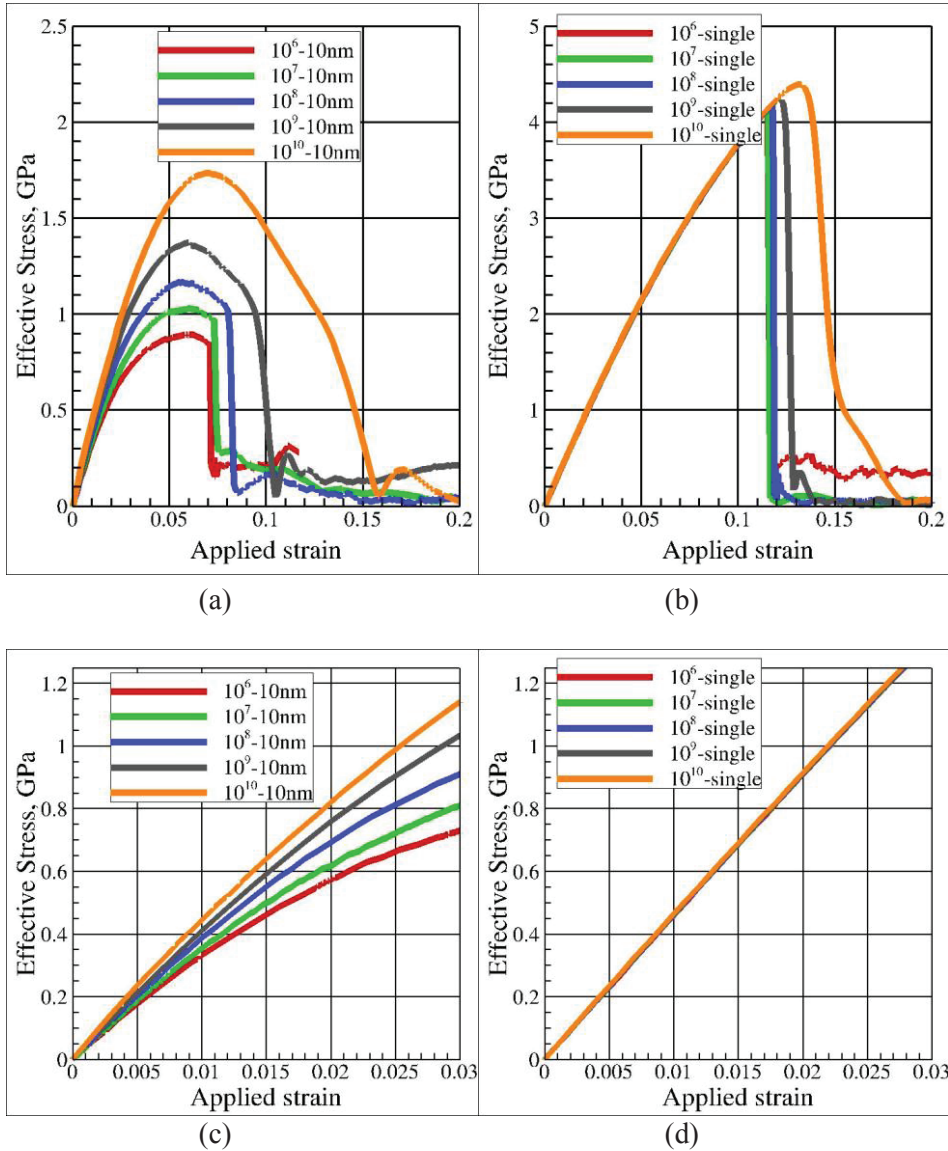

(a)

(b)

(c)

(d)

Figure 2: Strain rate effect on the evolution of the von Mises effective stress with respect to the applied strain. Figs. 2(a) and 2(c) show results for the 10 nm grain NCA atom system and Figs. 2(b) and 2(d) show results for the SCA atom systems.

The grains thus have pronounced effect on the range and average of the maximum values reached by σ_e at different strain rates. This effect starts from the very beginning in the applied straining process, as can be seen from the initial development of σ_e in the NCA system, see Figure 2(c). These results confirm the strong strain rate dependency of the initial σ_e development that was reported in literature at strain rates above 10^3 s^{-1} [Bodner, and Rajendran (1995)]. Several constitutive models have been proposed to incorporate the effects of strain rate on not only σ_e, but also on the initial yield stress. The initial σ_e in the NCA system (about 0.5 GPa in Figure 2(a)) is very low when compared to the initial σ_e in the SCA systems (well above 1.2 GPa in Figures 2(b) and 2(d)). These differences are attributed to the grain boundaries in the NCA microstructure that are responsible for the nucleation of dislocations. The SCA system, on the other hand, is clean and free of defects/grain boundaries. As a result, the SCA system deforms elastically for larger strains before the nucleation of dislocations. The deviation from linearity for the SCA system is attributed to the nucleation of dislocations, whereas the deviation from linearity in the NCA system is attributed to grain boundary sliding/rotation.

In Figures 3(a) and 3(b), σ_e is plotted with respect to the ε_p, instead of the total applied strain. The maximum σ_e in the NCA system is reached at plastic strains between 1% and 2% as can be seen in Figure 3(a). In the SCA systems, see Figure 3(b), the maximum σ_e is reached slightly above 4 GPa for plastic strains between 3% and 4%. The steep drop in σ_e beyond these strains is due to void nucleation and accumulation. Voids are observed to nucleate at the grain boundary triple junctions at these peak values of stress. Although the strains at void nucleation can be discerned form Figure 3(c) and 3(d) which show plots of V_f vs. ε_p for different strain rates for the NCA and SCA systems, respectively, there is difficulty in determining the exact ε_p values at which the void nucleation occurs and this is addressed at the end of the next section.

In the NCA system, the presence of grain boundaries causes the voids to nucleate at lower plastic strains. The nucleation of voids in the SCA systems is observed to occur at stacking fault intersections in the absence of grain boundaries. In other words, the nucleation process is delayed for higher strain rates for the SCA systems. These results from the atomistic simulations further confirm continuum models that assume that at very high strain rates, the ductility increases due to delay in damage nucleation under high inertial loading [Rajendran and Fyfe (1981)]. Due to intense void activities, material degrades leading to a substantial drop in the material strength as can be seen from Figure 3(a) and 3(b). An initially solid material becomes porous due to void nucleation and growth. In addition, the MD simulations further validate pressure dependency of the yield criterion, such as the one proposed by [Gurson (1977)] for porous metals. This aspect has been further addressed for
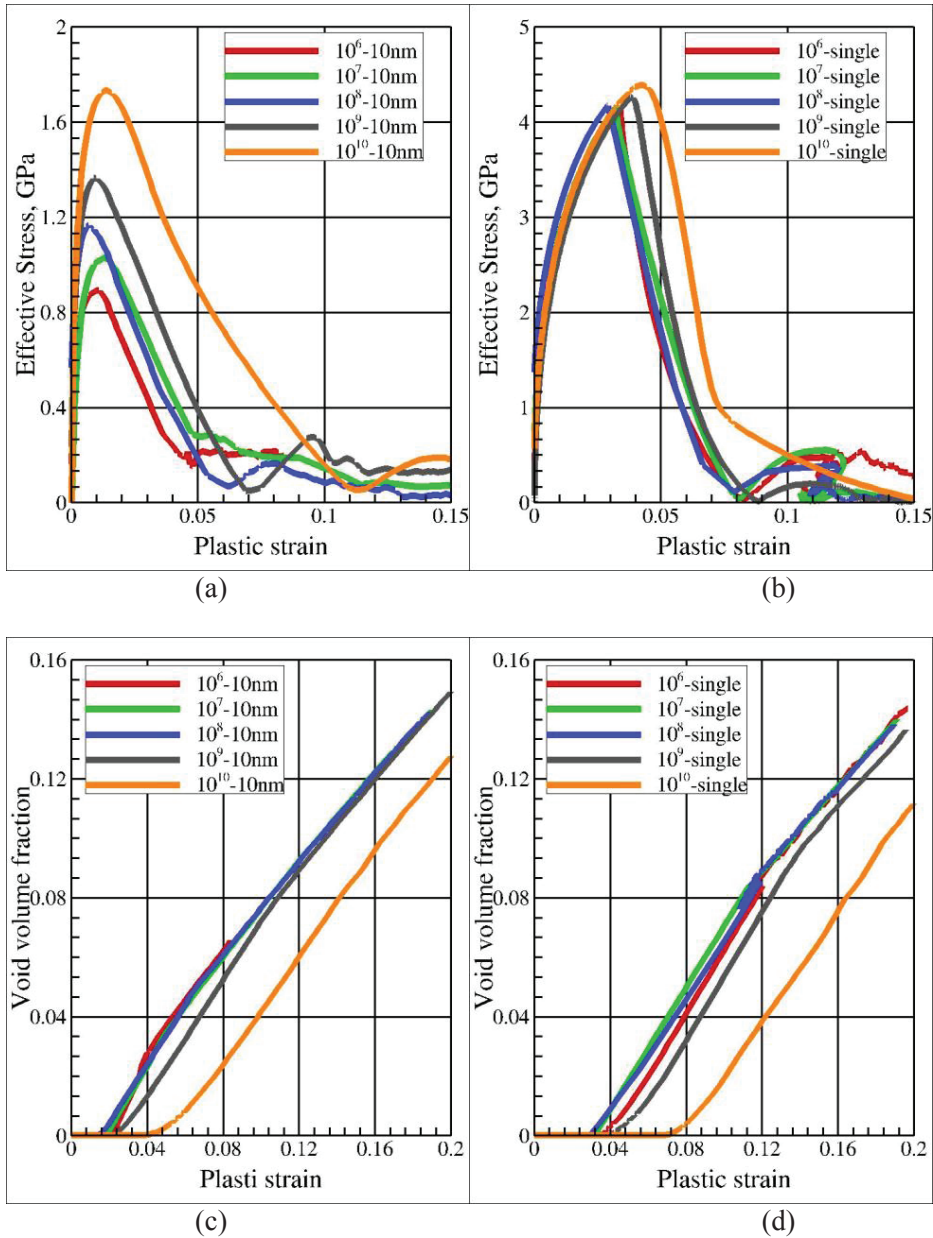
Figure 3: Strain rate effect on the evolutions of the effective stress, Figs. 3(a) and 3(b), and the void volume fraction, Figs. 3(c) and 3(d), with respect to the plastic strain. Figs. 3(a) and 3(c) show results for the 10 nm grain NCA atom system and Figs. 3(b) and 3(d) show results for the SCA atom systems.

copper by [Dongare, Rajendran, LaMattina, Zikry, and Brenner (2010b)].

Before the aspect of damage is discussed further, the effect of strain rate is summarized in Figure 4(a) on the peak values of the mean stress and in Figure 4(b) on the peak values of σ_e. The plots in Figure 4(b) clearly show that the peak σ_e dependence on the strain rate can follow some power law approximation for both the 10 nm grain NCA and SCA systems, much in the same manner as in the damage models for ductile materials in the continuum scale, [Gurson (1977)].
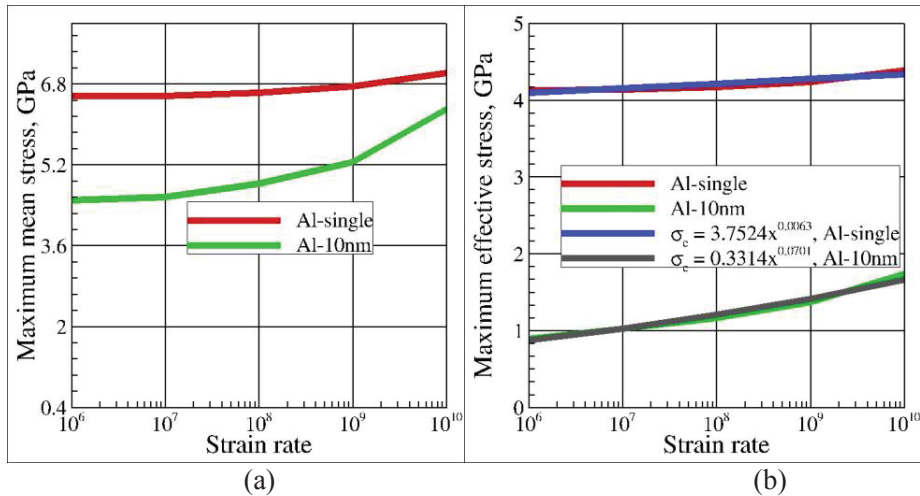

Figure 4: Strain rate effect on the maximum values of the mean and von Mises stresses for the 10nm grain NCA and SCA atom systems. Fig. 4(a) shows the results for the mean stress. Fig. 4(b) shows the results for the von Mises stress.

3.2 Void evolution

As discussed earlier, the dynamic failure of ductile materials under tensile loading is often controlled by voids nucleation and growth. For quantitatively determining the void evolution, the damage responses of V_f, ε_p and N_v are computed for each atom system, as discussed in Section 2.3. The appearance of voids and their growth are discussed only in terms of the V_f and N_v. The point at which a non-zero value appears for the V_f signifies an appearance of voids that are discernible by the particular method used in this work, not necessarily the actual void nucleation. Using a cube with a side length slightly above the aluminum lattice constant to map over the atom systems may miss finding voids that are not cubical in shape. Such voids may be expected, however, between the grains in the 10-nm NCA system or near

triple point GB junctions. Thus the void nucleation may be expected to have begun even earlier. A void should be defined as a case when two or more neighboring cells are empty; anything smaller than this cell will constitute a vacancy or a cluster of vacancies

The results for ε_p are presented in Figures 5(a) and 5(b) for the NCA and the SCA systems, respectively, as functions of the applied strain. The results for V_f are presented in Figures 6, while the results for N_v are presented in Figures 7.

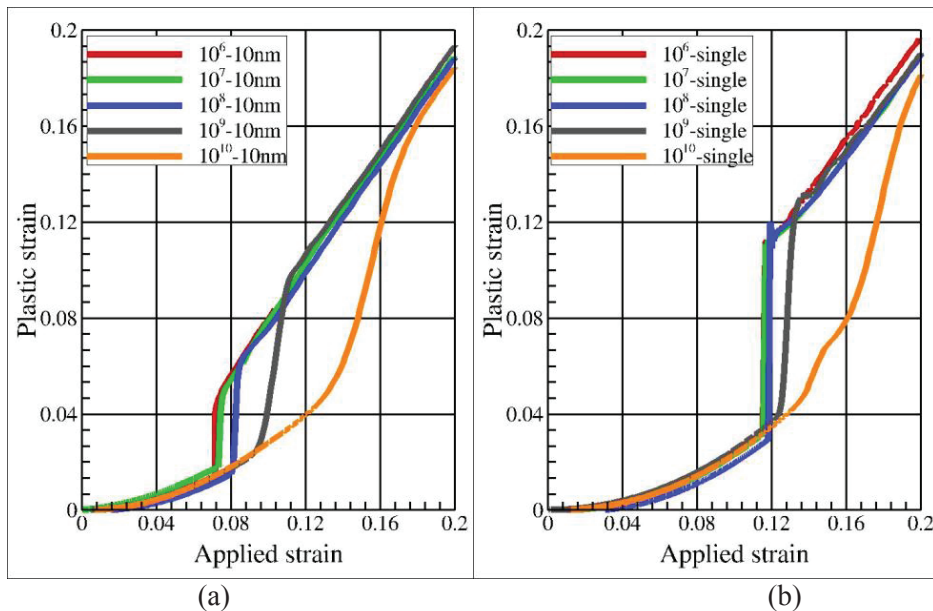<div align="center">(a)   (b)</div>

Figure 5: Strain rate effect on the evolution of the plastic strain with respect to the applied strain. Fig. 5(a) shows the results for the 10 nm grain NCA atom system. Fig. 5(b) shows the results for the SCA atom systems.

An initial gradual accumulation of ε_p can be seen from Figures 5(a) and 5(b) for both the NCA and SCA systems. This accumulation starts slowly from the very beginning of the applied strain, and doesn't show much sensitivity to the strain rate. Dislocations are seen as a cause for this initial ε_p accumulation. Dislocations cores appear and begin evolving into stacking faults, but formation of voids doesn't begin until towards the end of this phase, which is why Figures 6 show zero V_f and Figures 7 shows zero N_v, i.e., no void growth, for most part of the initial phase of ε_p accumulation.

The initial gradual accumulation of ε_p is followed by two stages of rapid growth in
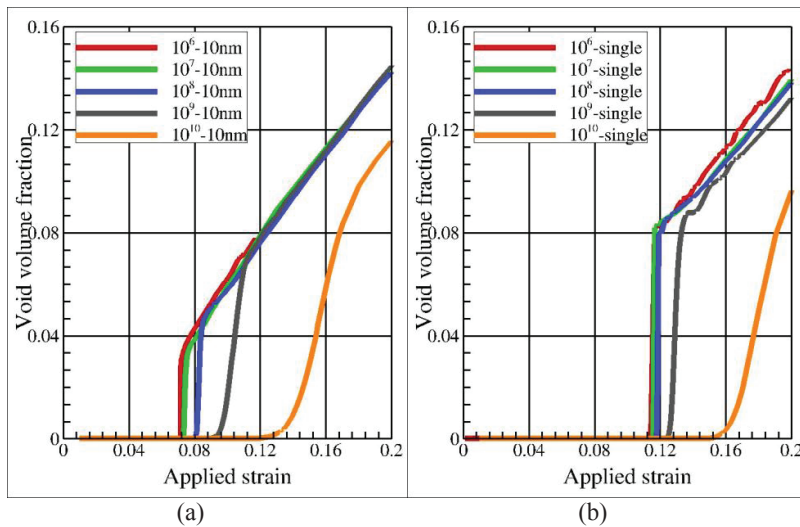
Figure 6: Strain rate effect on the evolution of the void volume fraction with respect to the applied strain. Fig. 6(a) shows the results for the 10 nm grain NCA atom system. Fig. 6(b) shows the results for the SCA atom systems.
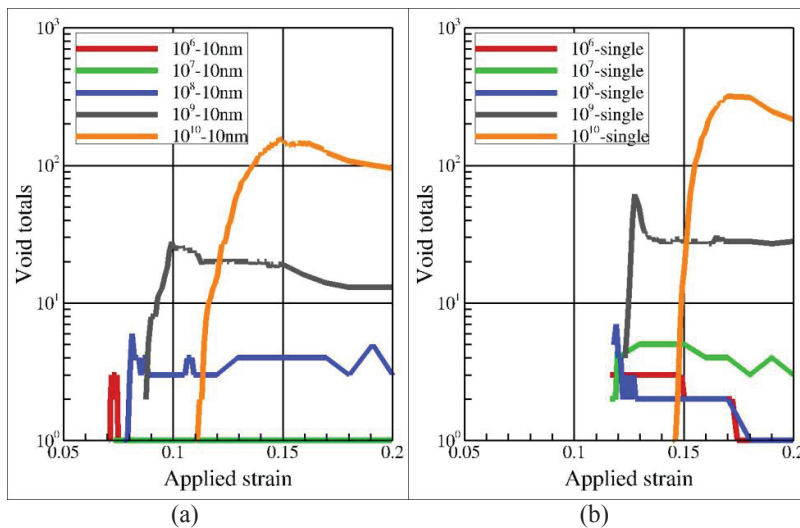

Figure 7: Strain rate effect on the evolution of the void totals with respect to the applied strain. Fig. 7(a) shows the results for the 10 nm grain NCA atom system. Fig. 7(b) shows the results for the SCA atom systems.

both ε_p and V_f. Based on the slope of ε_p with respect to the applied strain, Figures 5(a) and (5b) can be seen as showing that a major growth of ε_p is occurring in two stages. Similarly, Figures 6(a) and 6(b) can be seen as showing a concurrent and major growth of V_f, also occurring in two stages. In the following discussion, a correlation is shown between the two stages of the ε_p growth and the two stages of the V_f growth, and as a prelude to that discussion, these stages of growth are referred to as Stage I and Stage II of void growth.

During Stage I void growth increasing numbers of voids form and grow into physically discernible voids. With respect to the applied strain, the void nucleation and initial growth happens so quickly that V_f appears to rise very abruptly. Both the NCA and SCA systems show this trend especially for the lower strain rates of $10^6 \mathrm{s}^{-1}$ and $10^7 \mathrm{\ s}^{-1}$. During Stage II void growth, the larger numbers of voids begin to coalesce into smaller numbers and continue to grow.

Stage I void growth is characterized by two features: 1. void nucleation that is observed at the end of the initial ε_p accumulation continues into Stage I void growth, more numbers of smaller voids continue to form, and the total number of these smaller voids, i.e., N_v, continues to rise and peak. Stage II void growth begins with a drop in N_v which signifies the beginning of void coalescence. The larger numbers of smaller voids that appeared during Stage I void growth quickly coalesce into bigger voids and these voids continue to grow. Figures 7(a) and 7(b) which show N_v as functions of the applied strain for the NCA and the SCA systems, respectively, support this observation. As can be seen from these figures, initially one or two voids appear for the lower strain rates. For higher strain rates, multiple voids appear and their numbers rise very quickly reaching maximum values towards the end Stage I void growth. Higher void totals can be observed for the higher strain rates and for the SCA systems.

The applied strain range spanning the Stage I void growth is larger for the higher strain rates and for the SCA systems, and is small for the two smaller strain rates of $10^6 \mathrm{\ s}^{-1}$ and $10^7 \mathrm{\ s}^{-1}$ and for the NCA systems, as can be seen from the drops in the effective stress values in Figures 2 and 3, and from the sudden pick-up in the values of the ε_p and V_f in Figures 5and 6. Thus, with regards to the strain rate effect, the results in Figures 5-7 lend to two general observations. The first observation that can be made is that for the SCA systems the absence of grain boundary sliding makes for the stress harder to relax and for the large numbers of small voids harder to coalesce into some fewer larger ones until late in the applied straining process. The second observation is that the presence of grains in the NCA system makes available the grain boundary sliding as an additional mechanism for the initial void nucleation to take hold and voids to grow. Since this mechanism begins to have an effect early in the applied straining process, voids form very early on and have a

larger applied strain range to grow and coalesce. The fact that the N_v for the NCA system do not rise to the levels seen for the SCA systems confirms this, see Figures 7. By the end of the of the 20% applied strain range considered in this study, the N_v of the NCA system also come down roughly to 50% of the N_v's the SCA systems.
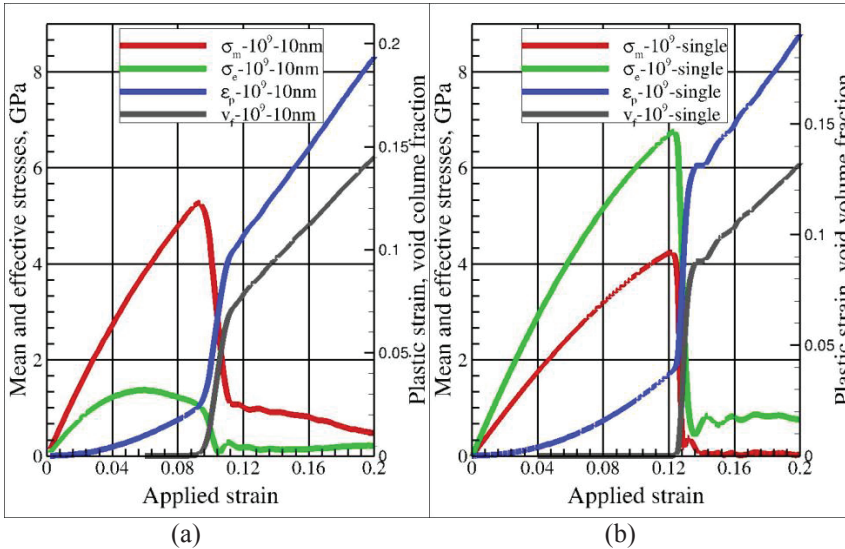

Figure 8: Evolutions of the mean stress, effective stress, plastic strain and void volume fraction with respect to the applied strain for the strain rate of $10^9 s^{-1}$. Fig. 8(a) shows the results for the 10 nm grain NCA atom system. Fig. 8(b) shows the results for the 1st SCA atom system. Scale on the left side of the plots is for the mean stress (σ_m) and the effective stress (σ_e). Scale on the right side of the plots is for the plastic strain (ε_p) and void volume fraction (V_f).

In order to show how the mean stress and flow stress are developing with respect to the different stages of development of the ε_p and V_f, results for the strain rate 10^9 s^{-1} are singled out for discussion. All the four results, i.e. the mean stress, σ_e, ε_p and V_f are plotted against the applied total strain in Figure 8(a) and 8(b) for the NCA and the SCA atom systems, respectively. The mean stress reaches its peak value just before the appearance of the voids and begins to drop as V_f and N_v increase, i.e. as Stage I void growth commences. The flow stress reaches its peak value much earlier than the mean stress. It reaches its peak value at ε_p values of 6% and 12%, respectively for the NCA and SCA systems. However, the estimated value for V_f continues to remain closer to zero at these strain levels. When ε_p increases to about 9% for the NCA system, V_f starts rapidly increasing to
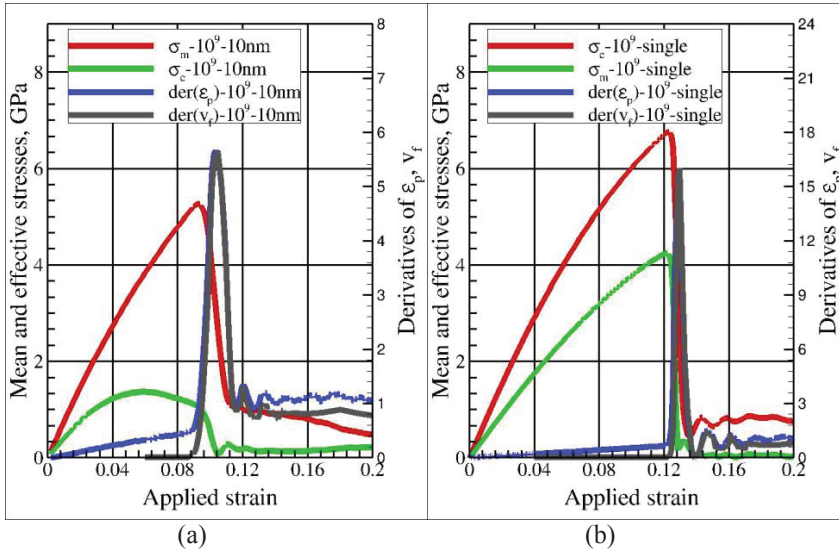
Figure 9: Evolutions of the mean stress, effective stress and derivatives of the plastic strain and void volume fraction for the strain rate of $10^9 s^{-1}$. Figs. 9(a) shows results for the 10 nm grain NCA atom system. Figs. 9(b) shows results for the 1st SCA atom system. Scale on the left side of the plots is for the mean stress (σ_m) and the effective stress (σ_e). Scale on the right side of the plots is for the derivatives of the plastic strain (ε_p) and void volume fraction (V_f) with respect to the applied strain.

6%. As the material softens due to voids accumulation, the flow stress falls rapidly to very low values and ε_p steeply increases from about 3% to 10%. However, in the SCA systems, the materials degrade rapidly at 12% strain while both ε_p and V_f instantaneously increase to 13% and 9% respectively.

In order to relate the changes in the mean and effective stresses to the gains in the ε_p and V_f, the derivatives of the ε_p and V_f are taken with respect to the applied strain and are plotted in Figure 9(a) and 9(b) for the NCA and the SCA atom systems, respectively. The derivative of ε_p is small and a shows a linear variation until Stage I void growth begins at which point the derivative ramps up quickly. The derivative value falls just as quickly as the Stage II void growth begins and continues nearly constant. The derivative of the V_f also shows a similar trend, but its value is zero for most of the initial phase of the ε_p accumulation. Rise in the V_f derivative value towards the end of the initial phase of ε_p accumulation indicates that some void nucleation has started. The derivative ramps up quickly as Stage I void growth
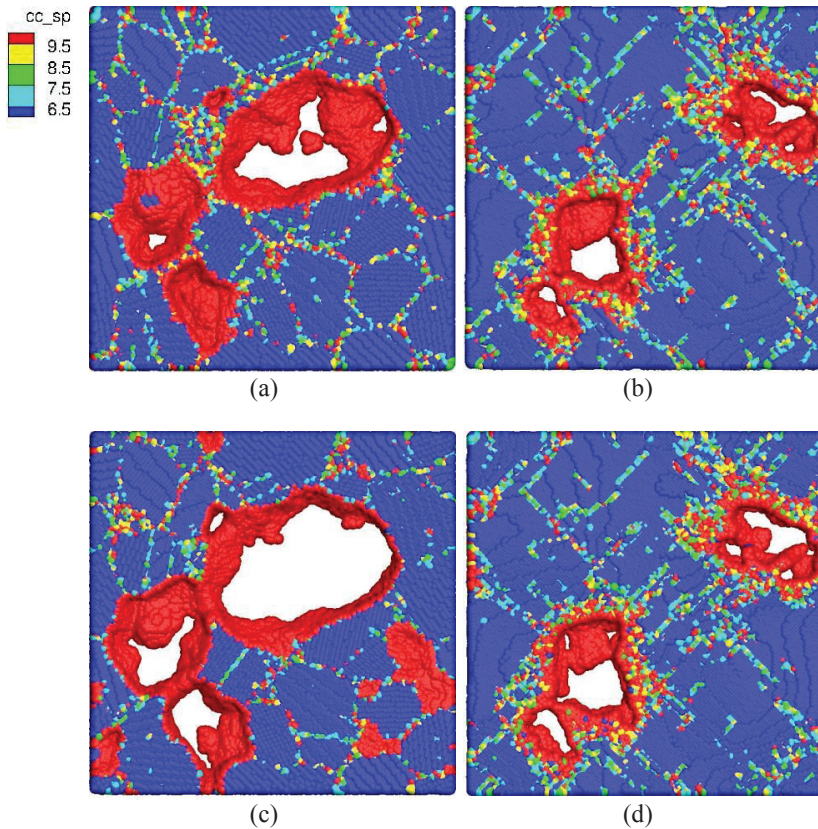
Figure 10: Growth of stacking faults into voids on some two sections of the atom systems at different strains applied under the strain rate $10^9 s^{-1}$. Figs. 10(a) and 10(c) show results for the 10 nm grain NCA atom system. Figs. 10(b) and 10(d) show results for the 1st SCA atom system. Atoms with CSP values in the range 6.5 to 9.5 are highlighted.

begins indicating further void nucleation and continuing growth of voids that are already formed. The transition from Stage I to Stage II of void growth is seen to occur at the peak value of the derivative of the V_f. At around these values, the smaller sized voids coalesce into bigger size voids and N_v begin to decrease signifying the critical void growth post major void coalescence.

It can be seen from the plots that the rates of accumulation for the ε_p during Stage I of void growth begin to lose the sensitivity to the strain rates. Evolutions of ε_p and V_f during Stage II void growth don't show much sensitivity to the strain rate for the
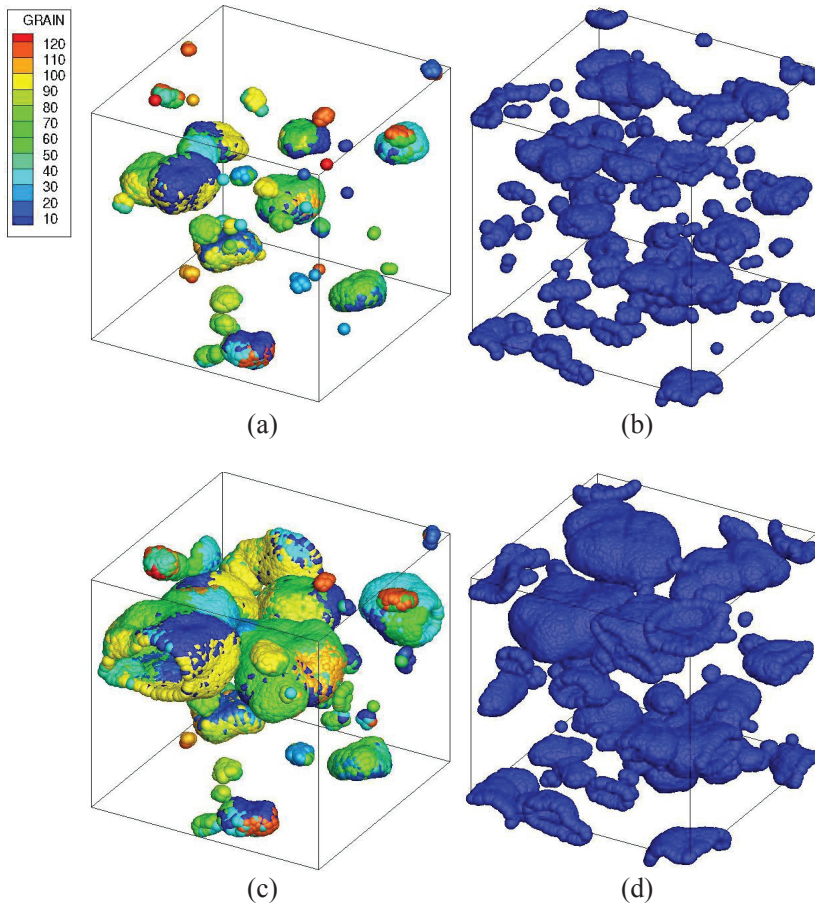
Figure 11: Situations of void growth at different strains applied under the strain rate $10^9 s^{-1}$. Figs. 11(a) and 11(c) show results for the 10 nm grain NCA atom system. Figs. 11(b) and 11(d) show results for the 1st SCA atom system. Atoms with CSP values < 20 are blanked.

strain rates considered in the study. The exception is the V_f evolution at the larger strain rate of 10^{10} s^{-1}, but even this sensitivity might disappear if the straining of the systems is continued past the 20% of the applied total strain considered in this study. Stage I void growth can thus be considered to span an applied strain range in which this void growth sensitivity to strain rate remains active. Previous MD simulations [Dongare, Rajendran, LaMattina, Zikry, and Brenner (2009b)] demonstrated similar void growth stages for nanocrystalline Cu with an average grain size

of 6 nm at a strain rate of 10^8 s^{-1}.

Following an initial gradual phase of ε_p accumulation, two stages of rapid plastic strain evolution are described and correlated with two stages of void growth so far. No attempt has been made in the present work to use the results for determining when exactly, i.e. with respect to the applied strain, the events of void nucleation, coalescence, and growth started and how starts of such events are affected by the strain rate and by the presence of the 10nm grain microstructure. To ascertain such events, one must investigate the deformed atomistic plots in addition to the ε_p and V_f, [Tsuru, and Shibutani (2004); Traiviratana, Bringa, Bensona, and Meyers (2008), Vo, Averback, Bellon, Odunuga, and Caro (2008); Dongare, Rajendran, LaMattina, Zikry, and Brenner (2010a)] .

In order to a give an idea of void coalescence and growth that can be observed from the present MD simulations, two snapshots of voids are provided on some sections of the atom systems in Figures 10 for the strain rate of 10^9 s^{-1}. The snapshots for the 10nm NCA system are provided in the left column of the figure, and for the SCA system in the right column of the figure. Similarly, in Figure 11, two snapshots of the void consolidation are provided. In Figure 10, atoms in the stacking faults are highlighted using a contour map of a parameter called the centrosymmetry parameter (CSP) [Kelchner, Plimpton, and Hamilton (1998)] in a range of 6.5 to 9.5. In Figure 11, the void surfaces are shown highlighting atoms with the CSP values > 20. Figures similar to 10 and 11 provide some understanding as to how voids are coalescing and growing into damage. Many void growth micromechanisms can be uncovered by a detailed investigation of such deformed atomistic plots. This work is currently underway and will be published shortly for all the three Al atom systems and for all the five strain rates considered in this study.

4   Conclusions

Until now, dynamic ductile failure, such as the spallation in a plate impact experiment under one dimensional strain state, has been modeled using empirical relationships for damage evolution [Gurson (1977); Needleman (1972); Tvergaard (1990); Tvergaard and Needleman (1984)]. The spallation process is dominated by the micromechanisms associated with voids nucleation, growth, and coalescence. The atomistic simulations provided further insight into the micromechanisms of the failure processes in the pure fcc aluminum. The lowest strain rate (10^6/sec) considered in this study was comparable to the strain rates typically measured in plate impact experiments. The stress–strain behaviors for a 10 nm nanocrystalline aluminum (NCA) atom system were compared with the behaviors of single crystal aluminum (SCA) systems at 5 different strain rates. Instantaneous loss of strength (flow stress) occurred in the NCA system at relatively low plastic strains (1% to

2%) for all the strain rates. However, the MD results indicated that increased ε_p is required to generate the same level of V_f in the SCA systems when compared to the NCA system. Because of the absence of grain boundaries, such as triple point grain boundary junctions in the SCA systems, the flow stress increased substantially to 4 GPa as compared to 1 GPa in the NCA system at the lowest strain rate.

The MD results further showed that a power law relationship could best describe the maximum flow stress dependence on the strain rate for both the NCA and SCA systems. The evolution of voids is also strongly dependent on the strain rates with larger number of voids forming in shorter amounts of times at higher strain rates. For the SCA system, a larger number of voids form initially as compared to the NCA system. These voids begin to coalesce at critical V_f values which are much higher for the SCA systems than for the NCA system.

Most continuum models use ad hoc empirical relationships to describe void nucleation and stable void growth. The present MD simulations revealed a two-phase void growth process: 1) disconnected voids are initially generated at a strain rate dependent first critical strain level which signifies the end of an initial slow ε_p accumulation, 2) individual voids continued to nucleate and grow until N_v peaked at a strain rate dependent second critical strain level, 3) the V_f jumped to higher values at this critical strain level, 4) at a strain rate dependent third critical strain level, voids began coalescing into a smaller numbers of void clusters showing stable void growth, and 5) a complete failure can be expected at third critical strain level. The plot of V_f versus ε_p revealed a complex two distinct slope based curve, while most or all continuum models seemed to have assumed a smooth curve.

The MD simulations revealed a highly strain rate dependent void nucleation, growth, and coalescence process in the NCA and the SCA atom systems. A better understanding of the micromechanisms of dynamic ductile failure may eventually lead to improved continuum failure models for crystalline materials.

References

Atluri, S.N.; Shen, S. (2002): The meshless local Petrov-Galerkin (MLPG) method: A simple and less-costly alternative to the finite element and boundary element methods. *Computer Modeling in Engineering & Sciences,* vol.3, no.1, pp. 11-51.

Bodner, S. R.; Rajendran, A. M. (1995): On the strain rate and temperature dependence of hardening of copper. AIP Conf. Proc. 370, pp. 499-502.

Bringa, E. M.; Caro, A.; Wang, Y.; Victoria, M.; McNaney, J. M.; Remington, B. A.; Smith, R. F.; Torralva, B. R.; Van Swygenhoven, H. (2005): Ultrahigh strength in nanocrystalline materials under shock loading. *Science,* vol. 309, pp. 1838-1841.

Curran, D.R.; Seaman, L.; Shockey, D.A. (1987): Dynamic failure of solids. *Phys. Rep.,* vol. 147, pp. 253-388.

Dong, L.; Atluri, S. N. (2012): Development of 3D T-Trefftz Voronoi Cell Finite Elements with/without Spherical Voids &/or Elastic/Rigid Inclusions for Microme-chanical Modeling of Heterogeneous Materials. *Comp. Mat. Continua,* vol. 29, no.2, pp. 169.

Dongare, A. M.; Rajendran, A. M.; LaMattina, B.; Zikry, M. A.; Brenner, D. W. (2008) Atomic scale simulations of orientation of loading axis on the growth of voids at the onset of ductile failure in single crystal Cu. *Mat. Res. Soc. Sym. Proc.,* vol. 1137, pp. EE08-09-W10-09.R1.

Dongare, A. M.; Rajendran, A. M.; LaMattina, B.; Zikry, M. A.; Brenner, D. W. (2009a): Atomistic studies of void-growth based spall failure in single crystal copper at high strain rates, Shock Compression of Condensed Matter - 2009. AIP Conference Proceedings. vol. 1195, pp. 769-772

Dongare, A. M.; Rajendran, A. M.; LaMattina, B.; Zikry, M. A.; Brenner, D. W. (2009b): Atomic scale simulations of ductile failure micromechanisms in nanocrystalline Cu at high strain rates. *Phys. Rev. B,* vol. 80, pp. 104108.

Dongare, A. M.; Rajendran, A. M.; LaMattina, B.; Zikry, M. A.; Brenner, D. W. (2010a): Atomic scale studies of spall behavior in nanocrystalline Cu. *J. Appl. Phys.*, vol. 108, pp. 113518.

Dongare, A. M.; Rajendran, A. M.; LaMattina, B.; Zikry, M. A.; Brenner, D. W. (2010b): Atomic scale study of plastic-yield criterion in nanocrystalline metals using molecular dynamics simulations. *Metall. Mater. Trans. A*, vol. 41A, pp. 523-531.

Dongare, A. M.; Rajendran, A. M.; LaMattina, B.; Zikry, M. A.; Brenner, D. W. (2011): Dynamic Failure behavior of Nanocrystaline Cu at atomic scales. *CMC,* vol. 24, no.1, pp.43-60.

Eliezer, S.; Gilath, I.; Bar-Noy, T. (1990): Laser-induced spall in metals: Experi-ment and simulation. *J. Appl. Phys.,* vol. 67, pp. 715.

Fowler, J. P.; Worswick, M. J.; Pilkey, A. K.; Nahme H. (2000): Damage leading to ductile fracture under high strain-rate conditions. *Metall. Mater. Trans. A* , vol. 31, pp. 831-844.

Gurson, A. L. (1977): Continuum theory of ductile rupture by void nucleation and growth: Part 1 – Yield Criteria and Flow rules for porous ductile. *J. Eng. Mater. Technol.,* Vol. 99, pp. 2-15.

Kanel, G. I.; Razorenov, S. V.; Utkin, A. V.; Fortov, V. E.; Baumung, K.; Karow, H. U.; Rusch, D.; Licht, V. (1993): Spall strength of molybdenum sin-

gle crystals. *J. Appl. Phys.,* vol. 74, pp. 7162.

Kanel, G. I.; Seaman, L,; Antoun, T; (2003): Spall Fracture, Springer-Verlag.

Knott, J. F. (1973): Fundamentals of Fracture Mechanics, Butterworths, London.

Kelchner, C.L.; Plimpton, S.J.; Hamilton, J.C.(1998): Dislocation nucleation and defect structure during surface indentation. *Phys Rev B,* vol.58, pp.11085.

Minich, R. W.; Cazamias, J. U.; Kumar, M.; and Schwartz, A. J. J. (2004): Effect of microstructural length scales on spall behavior of copper. Metall. *Mater. Trans. A,* vol. 35, pp. 2663-2673.

Meyers, M. A. (1994): *Dynamic Behavior of Materials.* Wiley-Interscience, New York.

Mishin, Y.;Farkas, D.; Mehl, M.J.; Papaconstantantopoulos, D.A.(1999): *Phys. Rev. B, vol.59, pp. 3393.* Al EAM in the LAMMPS setfl format. Conversion by C. A. Becker from Y. Mishin files. 30 December 2008. http://www.ctcms.nist.gov/potentials

Moshe, E.; Eliezer, S.; Dekel, E.; Ludmirsky, A.; Henis, Z.; Werdiger, M.; Goldberg, I. B.; Eliaz, N.; Eliezer, D. (1998): An increase of the spall strength in aluminum, copper, and Metglas at strain rates larger than 10^7 s^{-1}. *J. Appl. Phys.,* vol. 83, pp. 4004.

Moshe, E.; Eliezer, S.; Dekel, E.; Henis, Z.; Ludmirsky, A.; Goldberg, I. B.; Eliezer, D. (1999): Measurements of laser driven spallation in tin and zinc using an optical recording velocity interferometer system. *J. Appl. Phys.,* vol. 86, pp. 4242.

Needleman, A. (1972): Void growth in an elastic plastic medium. *J. Appl. Mech.*, vol. 39, pp. 964-970.

Plimpton, S. LAMMPS code 2011 version. http://lammps.sandia.gov/.

Rajendran, A. M.; Fyfe, I. M. (1982): Inertia Effects on the Ductile Failure of Thin Rings. *Appl. Mech, Trans. ASMR,* vol. 49, pp. 31-36.

Rajendran, A.M.; Dietenberger, M.A.; Grove, D. J.; (1989): *Results from the Recently Developed Dynamic Failure Model. Shock Compression of Condensed Matter-1989.* S.C. Schmidt, J.N. Johnson, and L.W. Davison (Editors), Elsevier Science Publishers, pp. 373-376.

Rivas, J. M.; Zurek, A. K.; Thissell, W. R.; Tonks, D. L.; Hixson, R. S. (2000): Quantitative description of damage evolution in ductile fracture of tantalum. *Metall. Mater. Trans. A,* vol. 31, pp. 845-851.

Seppala, E. T.; Belak J.; and Rudd, R.E.; (2004): Onset of void coalescence during dynamic fracture of ductile metals. *Phys. Rev. Lett.*, vol. 93, pp. 245503.

Seppala, E. T.; Belak, J.; Rudd, R.E. (2005): Three-dimensional molecular dy

namics simulations of void coalescence during dynamic fracture of ductile metals. *Phys. Rev. B,* vol. 71, pp. 064112.

Shen, S.; Atluri, S. N. (2004a): Computational nano-mechanics and multi-scale simulation. *Computers, Materials, & Continua*, vol.1, no.1, pp. 59-90.

Shen, S.; Atluri, S. N. (2004b): Atomic-level Stress Calculation and Continuum-Molecular System Equivalence. *CMES: Computer Modeling in Engineering & Sciences,* vol. 6, no. 1, pp. 91-104.

Tamura, H.; Kohama, T.; Kondo, K.; Yoshida, M. (2001): Femtosecond-laserinduced spallation in aluminum. *J. Appl. Phys.,* vol. 89, pp. 3520-3522.

Tewary, V.K.; Read, D.T. (2004): Integrated Green's function molecular dynamics method for multiscale modeling of nanostructures: application to Au nanoisland in Cu. *Computer Modeling in Engineering & Sciences,* vol.6, no.4, pp. 359-371.

Thomason, P. F. (1999): Ductile spallation fracture and the mechanics of void growth and coalescence under shock-loading conditions. *Acta Mater.,* vol. 47, pp. 3633-3646.

Traiviratana, S.; Bringa, E. M.; Bensona, D. J.; Meyers, M. A. (2008): Void growth in metals: Atomistic calculations. *Acta Mater.,* vol. 56, pp. 3874-3886 .

Tvergaard, V.; Needleman, A. (1984): Analysis of the cup-cone fracture in a round tensile bar. *Acta Metall.,* vol. 32, pp. 157-169.

Tvergaard, V. (1990): Material failure by void growth to coalescence. *Adv. Appl. Mech.,* vol. 27, pp. 83-151.

Tsuru, T.; Shibutani, Y. (2004): Atomistic simulations of elastic deformation and dislocation nucleation in Al under indentation-induced stress distribution. *Modelling Simul. Mater. Sci. Eng.*, vol.14, pp.S55–S62.

Vo, N. Q.; Averback, R. S.; Bellon, P.; Odunuga, S.; Caro, A. (2008): Quantitative description of plastic deformation in nanocrystalline Cu: Dislocation glide versus grain boundary sliding. *Phys. Rev. B,* vol. 77, pp. 134108.

Voter, A. F. (1994): *The Embedded Atom Method. In: Intermetallic Compounds: Principles and Practice.* Edited by J. H. Westbrook and R. L. Fleischer, Wiley, New York, pp. 77.

Wright, T. W.; Ramesh, K. T. (2008): Dynamic void nucleation and growth in solids: A self consistent statistical theory. *J. Mech. Phys. Solids,* vol. 56, pp.336 -359.

Xiong, L.; Chen, Y. (2008): Effects of dopants on the mechanical properties of nanocrystalline silicon carbide thin film. *Comp. Model. Engg. Sci.,* vol. 24, no.2/3, pp. 203.

Zhigilei, L. V.; Ivanov, D. S.; Leveugle, E.; Sadigh, B.; Bringa, E. M. (2004): Proc. SPIE vol. 5448, pp. 505.